Electronic Supplementary Material (ESI) for Dalton Transactions.
This journal is © The Royal Society of Chemistry 2017

SUPPORTING INFORMATION

Octahedral Yb(III) complexes embedded in $[Co^{III}(CN)_6]$-bridged coordination chains: combining sensitized near-infrared fluorescence with slow magnetic relaxation

Szymon Chorazy,[a,b] Michał Rams,[c] Junhao Wang,[b] Barbara Sieklucka,[a] and Shin-ichi Ohkoshi*[b]*

[a]*Department of Chemistry, School of Science, The University of Tokyo, 7-3-1 Hongo, Bunkyo-ku, Tokyo, 113-0033, Japan.*
[b]*Faculty of Chemistry, Jagiellonian University, Ingardena 3, 30-060 Krakow, Poland.*
[c]*Institute of Physics, Jagiellonian University, Łojasiewicza 11, 30-348 Krakow, Poland.*

*Corresponding authors: simon.chorazy@uj.edu.pl; ohkoshi@chem.s.u-tokyo.ac.jp

Experimental details. S2

Infrared absorption spectrum of **1** compared with the reference samples of $K_3[Co(CN)_6]$ and 3-hydroxypyridine. (Figure S1) S4

Thermogravimetric curve of **1** measured under an air atmosphere in the 20–370 °C temperature range, and the related comment. (Figure S2) S5

Crystal data and structure refinement for **1**. (Table S1) S6

Asymmetric unit of **1** with the atoms labelling scheme, and the resutling arrangement of atoms showing two isostructural fragments molecular buidling units differing in the orientation. (Figure S3) S7

Detailed structure parameters of **1**. (Table S2) S8

Results of Continuous Shape Measure (CSM) Analysis for $[Yb^{III}(3\text{-pyridone})_2(H_2O)_2(NC)_2]^+$ and $[Co^{III}(CN)_6]^{3-}$ complexes in **1**. (Table S3) S9

Detailed insight into the octahedral geometry of $[Yb^{III}(3\text{-pyridone})_2(H_2O)_2(NC)_2]^+$ and $[Co^{III}(CN)_6]^{3-}$ complexes of **1**. (Figure S4) S9

The supramolecular arrangement of cyanido-bridged chains of **1** with the insight into details of hydrogen bonding network. (Figure S5) S10

Powder X-ray diffraction pattern of the polycrystalline sample of **1**. (Figure S6) S11

Zero-field cooled and field cooled magnetization curves of **1** in the 1.8–20 K range at H_{dc} = 20 Oe. (Figure S7) S12

Alternate-current (*ac*) magnetic properties of **1** under zero direct-current (*dc*) magnetic field. (Figure S8) S12

The dependence of in-phase (χ_M') and out-of-phase (χ_M'') molar magnetic susceptibilities on the applied *dc* magnetic field from the 0–3000 Oe range at H_{ac} = 1 Oe and various indicated temperatures. (Figure S9) S13

Ac magnetic properties of **1** under *dc* field of 1000 Oe. (Figure S10) S14

Parameters obtained by fitting the Argand χ_M''–χ_M' plots (H_{dc} = 1000 Oe) of **1** using the generalized Debye model. (Table S4) S15

Temperature dependence of the inverse of the determined relaxation time of **1** together with the possible fittings taking into account various relaxation processes. (Figure S11) S16

Solid state UV-Vis-NIR absorption spectra of **1** compared with the spectra of 3-pyridone and $K_3[Co(CN)_6]$. (Figure S12) S17

Analysis of solid state UV-Vis-NIR absorption spectrum of **1** compared with the analyses of the relevant spectra of 3-pyridone and $K_3[Co^{III}(CN)_6]$. (Table S5) S18

Room temperature solid state excitation (left panel) and emission (right panel) spectra of **1** compared with the respective spectra of 3-pyridone and $K_3[Co(CN)_6]$. (Figure S13) S19

Summary of structural features, magnetic and optical properties of reported cyanido-bridged heterometallic assemblies containing Yb^{III} complexes. (Table S6) S20

References to Supporting Information. S22

Experimental details.

Materials

Ytterbium(III) chloride hexahydrate ($Yb^{III}Cl_3·6H_2O$, CAS: 10035-01-5), 3-pyridone (3-hydroxypyridine, 3-pyridinol, CAS: 109-00-2), and potassium hexacyanocobaltate(III) ($K_3[Co^{III}(CN)_6]$, CAS: 13963-58-1) were purchased from commercial sources (Sigma-Aldrich), reagent grade, and used without purification.

Synthesis and basic characterization of 1

The 0.18 mmol (60.0 mg) portion of $K_3[Co^{III}(CN)_6]$ was dissolved in the 0.75 mL of distilled water to get solution I. Then, the 0.18 mmol (69.8 mg) portion of $Yb^{III}Cl_3·6H_2O$, and the 0.36 mmol (34.5 mg) portion of 3-pyridone were dissolved together in the small amount (0.75 mL) of distiller water. The resulting white suspension was stirred with continuous heating to the boiling point to obtain the clear colourless solution II. After that, the hot solution II was quickly added to the solution I, and the resulting white suspension was vigorously stirred for a few seconds, and filtrated. It resulted in the clear colourless solution which was closed and left undisturbed for crystallization. The colourless block crystals of **1** started to appear after a few minutes. The whole crystalline product was collected by the suction filtration after one day. The crystals of **1** were washed by a small amount of cold water, and heavily by ethanol which was followed by drying the crystals on the air. The resulting crystalline material is stable on the air, and can be identified by the composition of $\{[Yb^{III}(\text{3-pyridone})_2(H_2O)_2][Co^{III}(CN)_6]\}$ (**1**) as found by the single-crystal X-ray diffraction, and confirmed by the CHN analysis, IR spectra (Figure S1), and thermogravimetric studies (Figure S2). Yield: 32 mg, 29%.

IR spectrum (KBr, cm^{-1}, Figure S1). CN^- stretching vibrations: 2151w, 2137sh, 2131vs, 2120vs, indicated the presence of $[Co^{III}(CN)_6]^{3-}$ ions existing both in bridging and terminal modes (Figure S1b).[S1-S4] A number of peaks in the 1500–700 cm^{-1} correspond to the various vibrational modes of 3-pyridone. They are also observed in the pure 3-hydroxypyridine (3-pyridone) but their positions are variously shifted in **1** due to the coordination of this ligand to Yb^{III}.[S5-S6]

CHN elemental analysis. Anal. Calcd. for $Yb_1Co_1C_{16}H_{14}N_8O_4$ (**1**, M_W = 614.31 $g·mol^{-1}$): C, 31.28%; H, 2.30%; N, 18.24%. Found: C, 31.20%; H, 2.36%; N, 18.23%. TGA (Figure S2): loss of 2 H_2O per Yb-Co pair, calcd. 5.9%, found, 6.3%.

Crystal structure determination

Single crystal X-ray diffraction experiment for 1 was conducted using a Rigaku R-AXIS RAPID diffractometer with imaging plate area detector and graphite monochromated Mo Kα radiation. The well-shaped single crystal was taken from the solution, dispersed in a paratone-N oil, mounted on Micro Mounts™ holder, and measured at the low temperature of 100(2) K (Table S1). The crystal structure was solved by a direct method using SHELXS-97, and refined by a full-matrix least squares technique using SHELXL-2014/7.[S7] Calculations were executed using partially Crystal Structure crystallographic software package, and partially WinGX (v2014.1) integrated system.[S8] All non-hydrogen atoms were refined anisotropically. The hydrogen atoms were found independently from the electron density map. Among them, the hydrogen atoms of water molecule, attached to O2 atom, and the hydrogen atom of NH group, attached to N5, were refined isotropically using a riding model, and their distances to the related heavy atoms of O2/N5 were fixed using a DFIX command. All other hydrogen atoms were refined isotropically without any restraints. Due to the non-negligible structural disorder around O atoms attached to Yb, and C1/N1 atoms of cyanide ligand, some restraints on the thermal ellipsoids (DELU, ISOR) of the related atoms were applied to ensure to convergence of the refinement process. It is important to note that the hydrogen atom (H5N) attached to the N5 atom was found from the electron density map suggesting the predominant 3-pyridone tautomeric form of the applied organic ligand, while the alternative hydrogen atom attached to O1, that could have suggested the 3-hydroxypyridine form of the organic ligand, could not be found. This indicated that in **1**, the most probable form of the organic ligand is 3-pyridone rather than 3-hydroxypyridine.[S9] Structure diagrams were prepared using Mercury 3.5.1 software.[S10] CCDC reference number for the crystal structure of **1** is 1550695.

Physical techniques

Infrared spectrum of **1** was measured on the single crystals using a Nicolet iN10 MX FTIR microscope, settled in a transmission method, while infrared spectra of the reference materials were measured on the polycrystalline samples mixed and pressed with KBr using a Jasco FTIR-4100 spectrometer. The UV-Vis-NIR diffuse reflectance spectra were measured using a Jasco V-670 spectrophotometer on a polycrystalline sample grinded with barium sulphate. Thermogravimetric curve was collected on a Rigaku Thermo Plus TG8120 in the 20–370 °C range under an air atmosphere with a heating rate of 1 $°C\cdot min^{-1}$. Elemental analysis of C, H, and N were performed using an EuroEA EuroVector elemental analyser. Powder X-ray diffraction pattern of the polycrystalline sample of **1** was collected on a Rigaku Ultima-IV with Cu Kα radiation.

Photoluminescent properties, including emission and excitation spectra were measured on a Horiba Jobin-Yvon Fluorolog-3 (FL3-211) spectrofluorimeter (model TKN-7) equipped with an Xe (450 W) lamp as an excitation source with a room-temperature R928P emission detector working in a photon-counting mode. The background correction and the further analyses were performed using a Fluoressence software. The luminescent measurements were executed at room temperature in the standard solid-state holder. Magnetic studies were performed using a Quantum Design MPMS XL magnetometer on the polycrystalline samples submerged in a paraffin oil to avoid the rotation of crystals under an applied magnetic field. The diamagnetic contributions from the sample, oil, and the holder were estimated and subtracted.

Calculations

Continuous Shape Measure Analysis for coordination spheres of six-coordinated Yb^{III} and Co^{III} complexes of **1** was performed using SHAPE software ver. 2.1.[S11-S12]

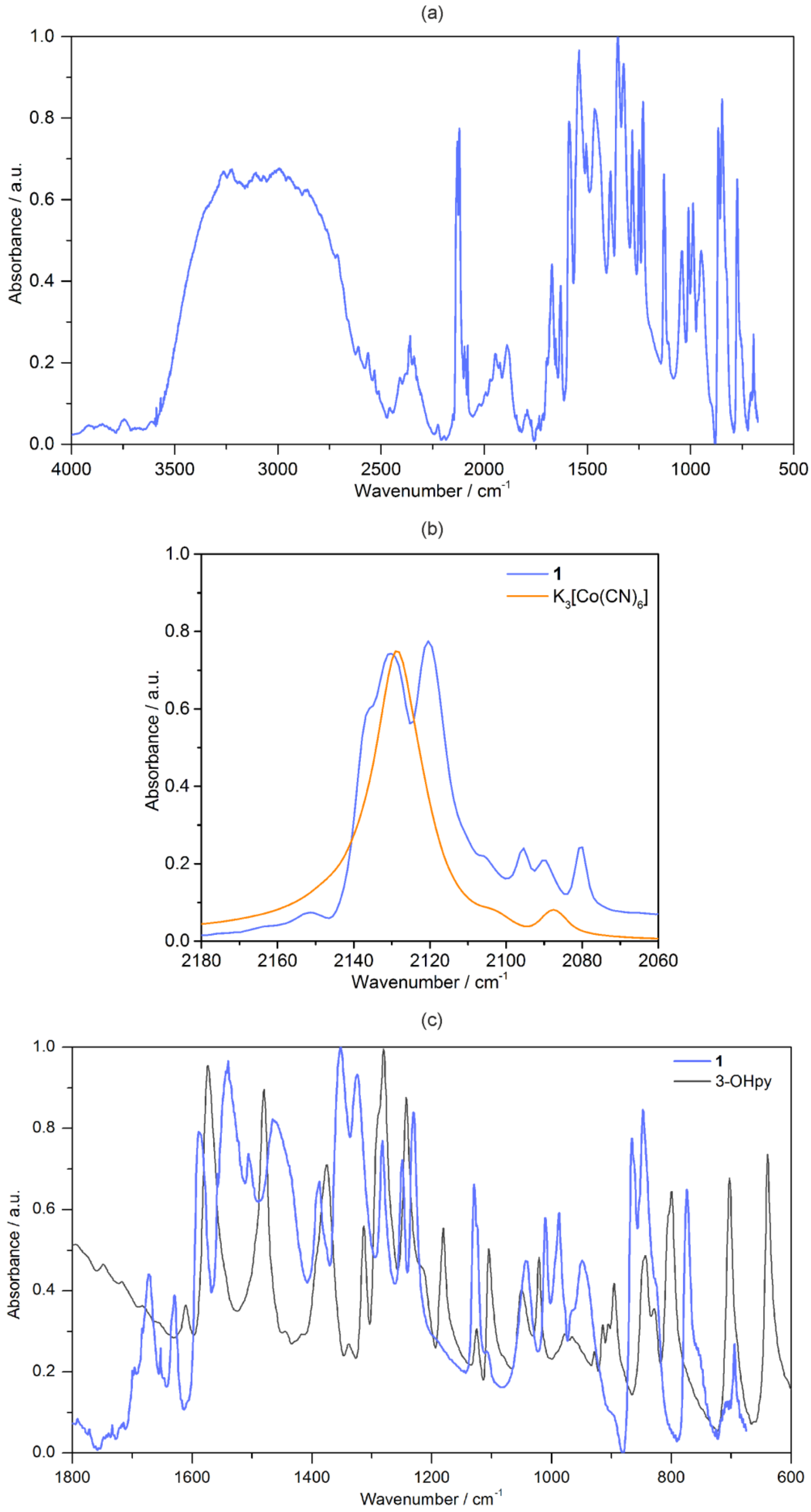

Figure S1. Infrared absorption spectrum of **1** (blue line) in the full 4000–600 cm^{-1} range (*a*), compared with the $K_3[Co(CN)_6]$ salt (orange line) in the limited 2180–2060 cm^{-1} related to the stretching vibrations of cyanides (*b*), and compared with 3-hydroxypyridine (dark grey line) in the limited 1800–600 cm^{-1} (*c*).

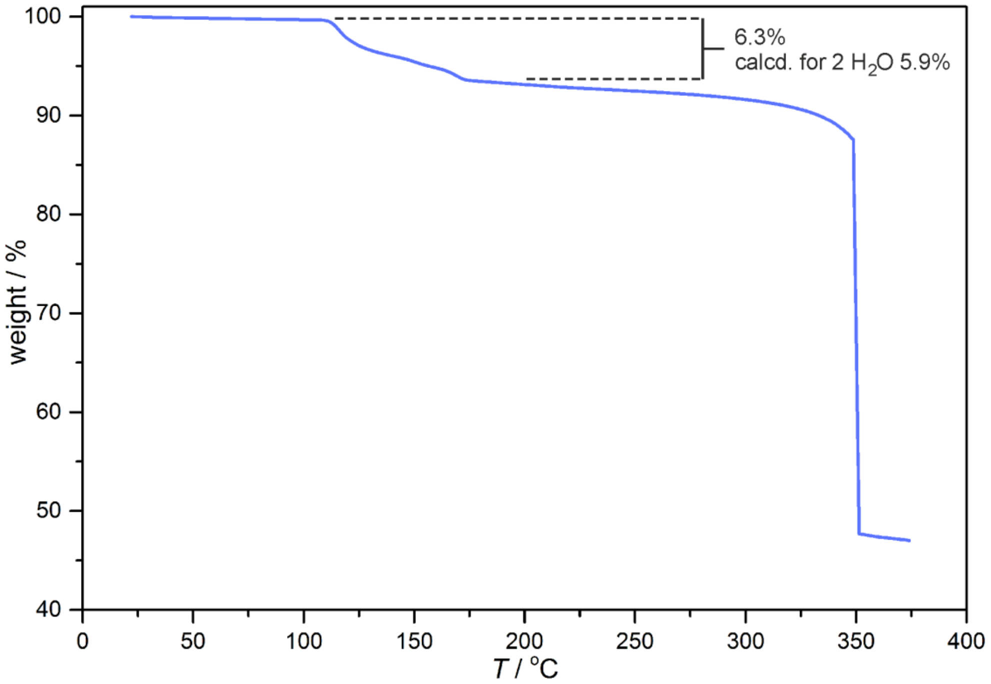

Figure S2. Thermogravimetric curve of **1** measured under an air atmosphere in the 20–370 °C temperature range with the two indicated steps related to loss of water molecules (see comment below).

Comment to Figure S2:

On heating from room temperature to ca. 110°C, **1** reveals almost a stable composition without noticeable decrease of the mass. On further heating, the gradual decrease of the mass to ca. 94.1% in the range of 110–170°C is observed. The related weight loss by the value of 6.3% corresponds reasonably to the removal of two coordinated water molecules per one {$Yb^{III}Co^{III}$} unit (calculated weight loss of 5.9%). Thus, the indicated step in the TGA curve is a good agreement with the composition of **1**, {[Yb^{III}(3-pyridone)$_2$(H_2O)$_2$][Co^{III}(CN)$_6$]}, determined by the CHN elemental analysis. The dehydrated phase of the presumable formula {[Yb^{III}(3-pyridone)$_2$][Co^{III}(CN)$_6$]}, seems to be quite stable as above 170°C a long plateau is observed almost up to 340°C. At the highest temperatures, the mass of **1** dramatically decreases reaching only 47% of the starting value at 375°C.

Table S1. Crystal data and structure refinement for **1**.

Compound		**1**
method		single-crystal XRD
formula		$Dy_1Co_1C_{16}H_{14}N_8O_4$
formula weight [g·mol^{-1}]		614.32
T [K]		100(2)
λ [Å]		0.71075 (Mo Kα)
crystal system		monoclinic
space group		C 2/m (no. 12)
unit cell	$\boldsymbol{a}$ [Å]	10.5773(5)
	$\boldsymbol{b}$ [Å]	13.5743(6)
	$\boldsymbol{c}$ [Å]	8.8978(4)
	$\boldsymbol{\alpha}$ [deg]	90
	$\boldsymbol{\beta}$ [deg]	125.244(9)
	$\boldsymbol{\gamma}$ [deg]	90
V [Å^3]		1043.37(13)
Z		2
calculated density [g·cm^{-3}]		1.955
absorption coefficient [cm^{-1}]		5.289
F(000)		590
crystal shape and colour		colourless block
crystal size [mm × mm × mm]		0.13 × 0.10 × 0.07
Θ range [deg]		3.001 – 27.416
limiting indices		$-13 < h < 13$ $-17 < k < 15$ $-11 < l < 11$
collected reflections		5073
unique reflections		1236
R_{int}		0.0156
completeness [%]		99.7
max. and min. transmission		0.546 and 0.708
refinement method		full-matrix least-squares on F^2
data/restraints/parameters		1236/11/160
GOF on F^2		1.452
final R indices		$R_1 = 0.0105$ [$I > 2\sigma(I)$] $wR_2 = 0.0421$ (all data)
largest diff peak and hole		0.731 and -0.867 e·A^{-3}

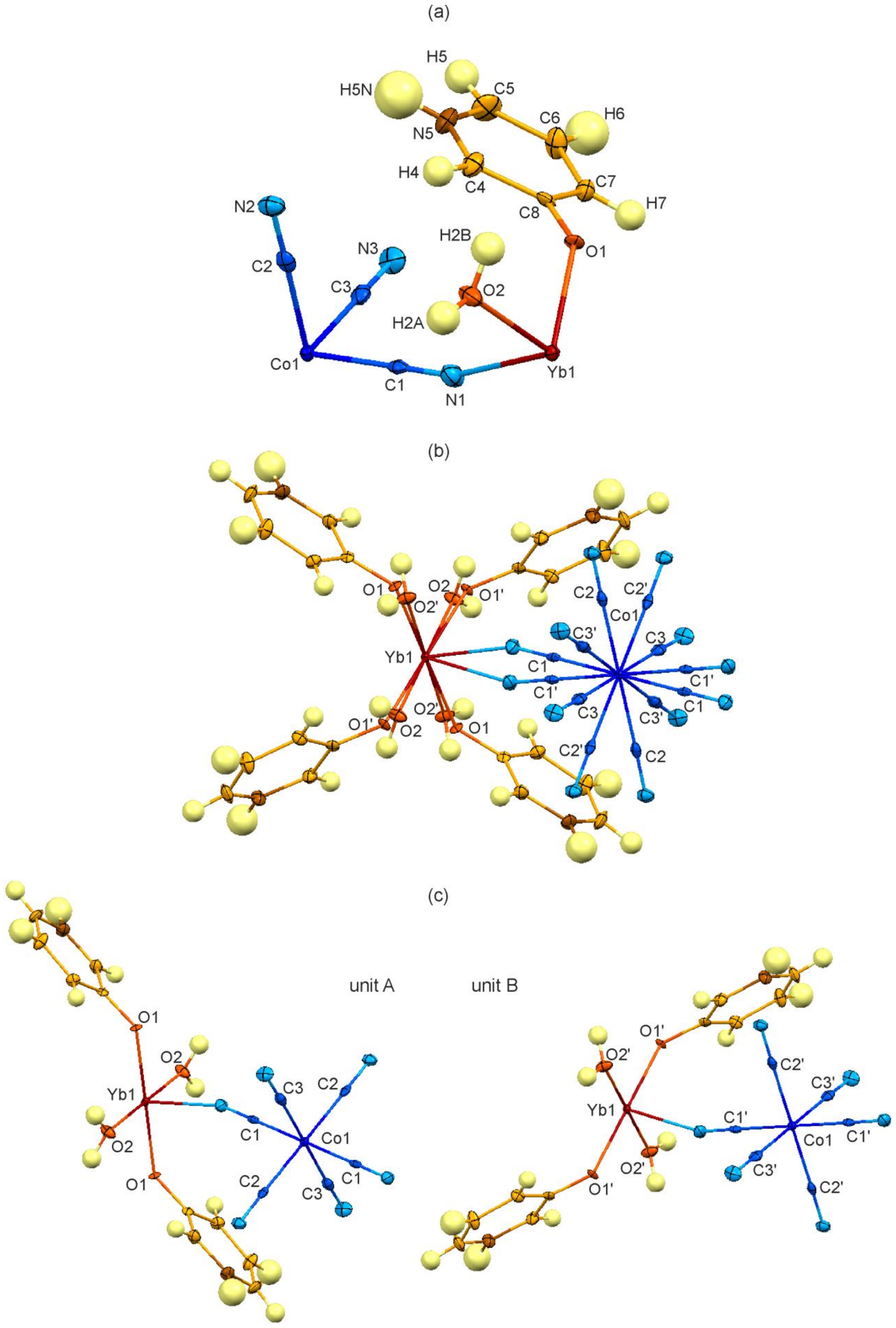

Figure S3. Detailed structural views of **1**: asymmetric unit with the atoms labelling scheme (*a*), the resulting arrangement of atoms in the representative fragment of the structure (*b*) showing two isostructural molecular building units (A and B) differing in the orientation (*c*), with all the atoms of 0.5 site occupancies. The atoms within the fragment A are generated by the inversion centres situated on the metal atoms, while the fragment B is produced from the fragment A by the mirror plane lying within *ac* plane. Atoms are shown with 60% probability level.

Table S2. Detailed structure parameters of **1**.

Details of $[\mathrm{Yb^{III}(3\text{-pyridone})_2(H_2O)_2(NC)_2}]^{+}$ complex		Details of $[\mathrm{Co^{III}(CN)_6}]^{3-}$ complex	
Parameter	Value [Å, °]	Parameter	Value [Å, °]
Yb1-O1	2.157(4)	Co1-C1	1.878(5)
Yb1-O2	2.222(5)	Co1-C2	1.898(6)
Yb1-N1	2.231(5)	Co1-C3	1.901(6)
Yb1-N1-C1	161.3(4)	C1-N1	1.153(7)
Yb1-O1-C8	137.4(4)	C2-N2	1.147(8)
N1-Yb1-N1	180	C3-N3	1.150(8)
O1-Yb1-O1	180	Co1-C1-N1	178.2(5)
O2-Yb1-O2	180	Co1-C2-N2	178.9(5)
N1-Yb1-O1	89.31(17), 90.69(17)	Co1-C3-N3	178.0(5)
N1-Yb1-O2	89.19(18), 90.81(18)	C1-Co1-C1	180
O1-Yb1-O2	89.0(2), 91.0(2)	C2-Co1-C2	180
O1-C8 (3-pyridone)	1.332(7)	C3-Co1-C3	180
C4-C8 (3-pyridone)	1.406(8)	C1-Co1-C2	90.0(2), 90.0(2)
N5-C4 (3-pyridone)	1.347(8)	C1-Co1-C3	88.4(2), 91.6(2)
C5-N5 (3-pyridone)	1.347(8)	C2-Co1-C3	89.8(2), 90.2(2)
C6-C5 (3-pyridone)	1.367(9)	Co1-Yb1 (C1-N1 bridge)	5.289
C7-C6 (3-pyridone)	1.383(8)		
C7-C8 (3-pyridone)	1.382(8)	Yb1-Yb1’	10.577

Hydrogen bonding network			
Parameter	Value [Å]	Parameter	Value [Å]
N2-(H2B)-O2	2.732	O1-(H5N)-N5	2.879
N3-(H2A)-O2	2.716		

Table S3. Results of Continuous Shape Measure (CSM) Analysis for $[\mathrm{Yb^{III}(3\text{-}pyridone)_2(H_2O)_2(NC)_2}]^+$ and $[\mathrm{Co^{III}(CN)_6}]^{3-}$ complexes in **1**.

Parameter	$[\mathrm{Yb^{III}(3\text{-}pyridone)_2(H_2O)_2(NC)_2}]^+$	$[\mathrm{Co^{III}(CN)_6}]^{3-}$
CSM parameter for hexagon (D_{6h})[S11-S12]	32.940	32.658
CSM parameter for pentagonal pyramid (C_{5v})	29.772	29.987
CSM parameter for octahedron (O_h)	**0.114**	**0.016**
CSM parameter for trigonal prism (D_{3h})	16.539	16.534

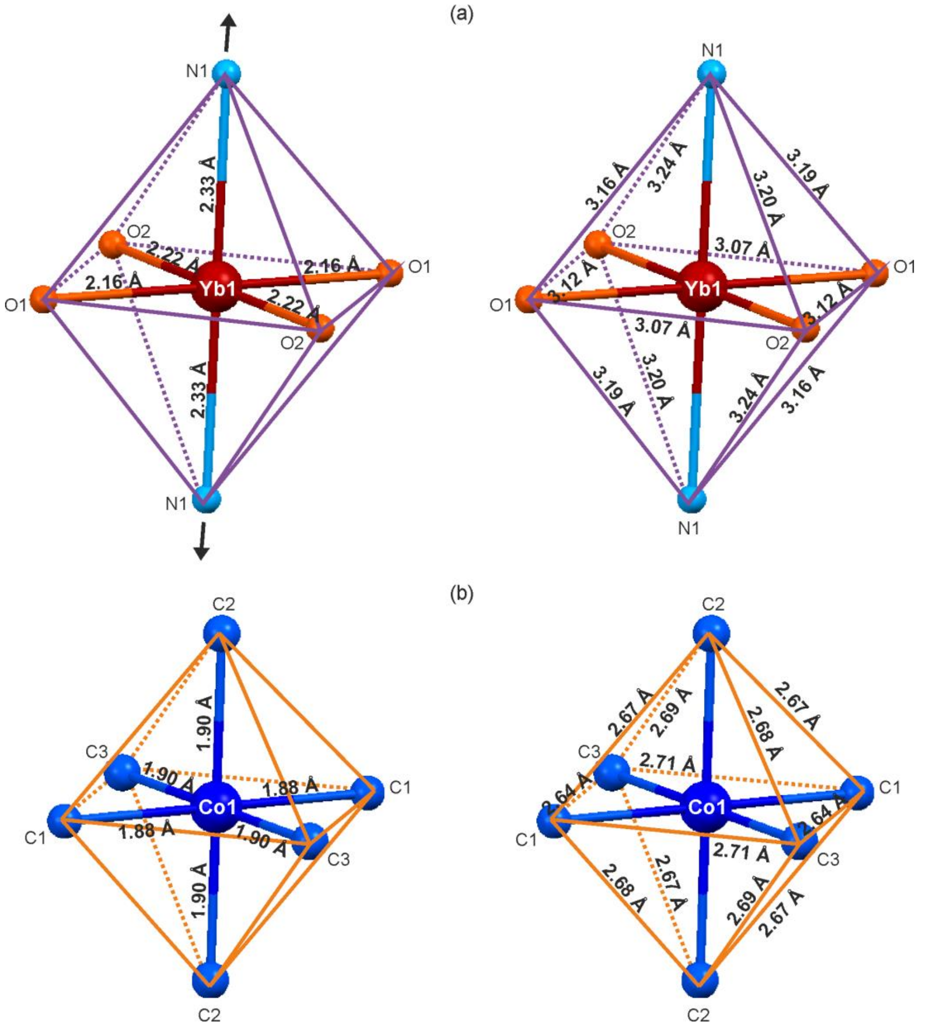

Figure S4. Detailed insight into the octahedral geometry of $[\mathrm{Yb^{III}(3\text{-}pyridone)_2(H_2O)_2(NC)_2}]^+$ (*a*) and $[\mathrm{Co^{III}(CN)_6}]^{3-}$ (*b*) complexes of **1**: the arrangement of bond lengths within the polyhedron with the indicated elongation directions (left panel), and the detailed dimensions of the polyhedrons (right panel).

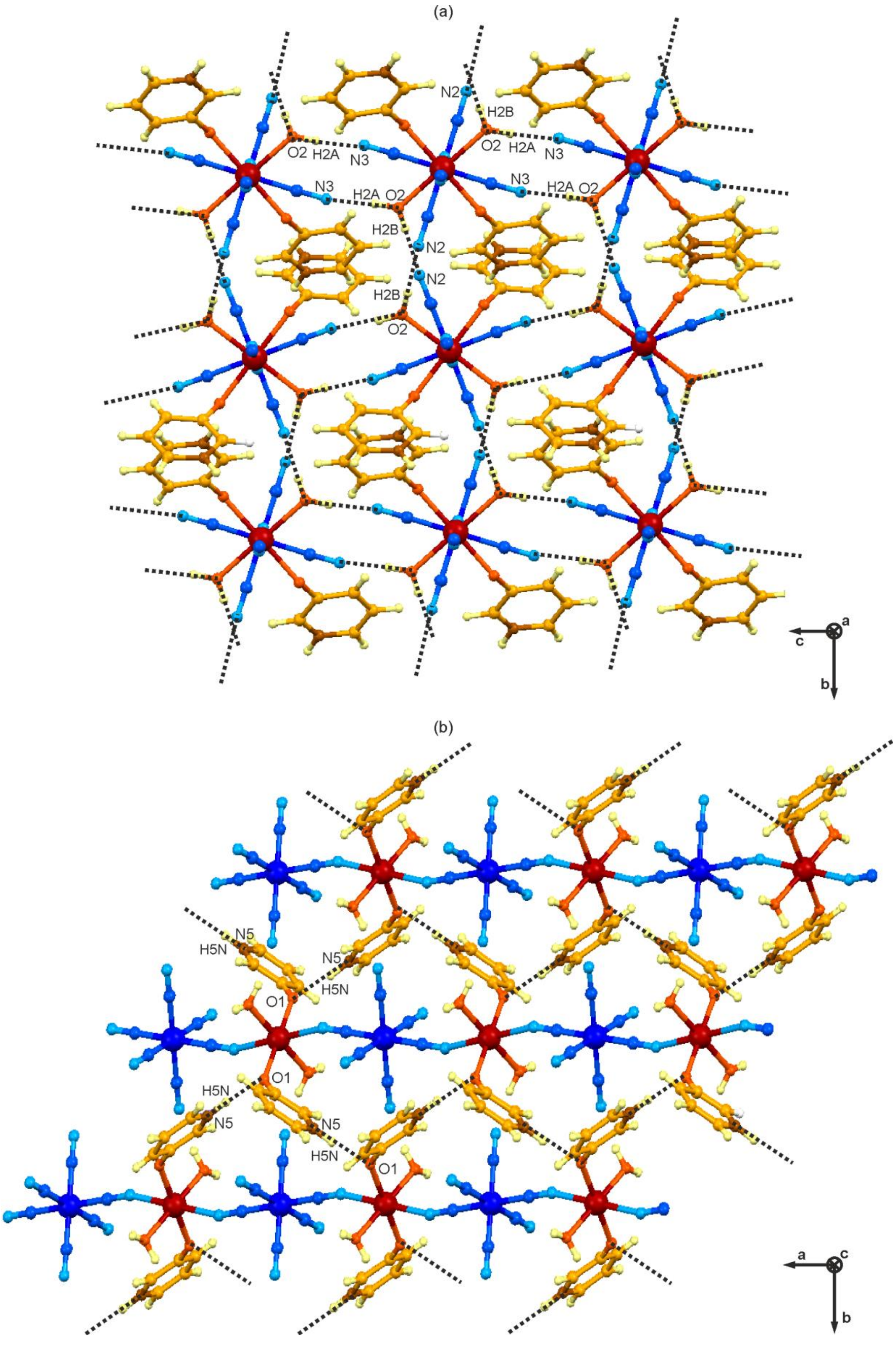

Figure S5. The supramolecular arrangement of cyanido-bridged chains of **1** with the insight into details of hydrogen bonding network involving water molecules bonded to terminal cyanides of neighbouring chains (*a*), and NH groups of 3-pyridone ligands bonded to oxygen atoms of 3-pyridone ligands of neighbouring chains (*b*). The hydrogen bonds are presented as dotted lines. The interatomic distances related to the presented hydrogen bonds are gathered in Table S2. Colours: Yb, dark red; Co, dark blue; C of cyanides, blue; N of cyanides, light blue; O of water, deep orange; C of 3-pyridone, orange; N of 3-pyridone, brown; H, yellow.

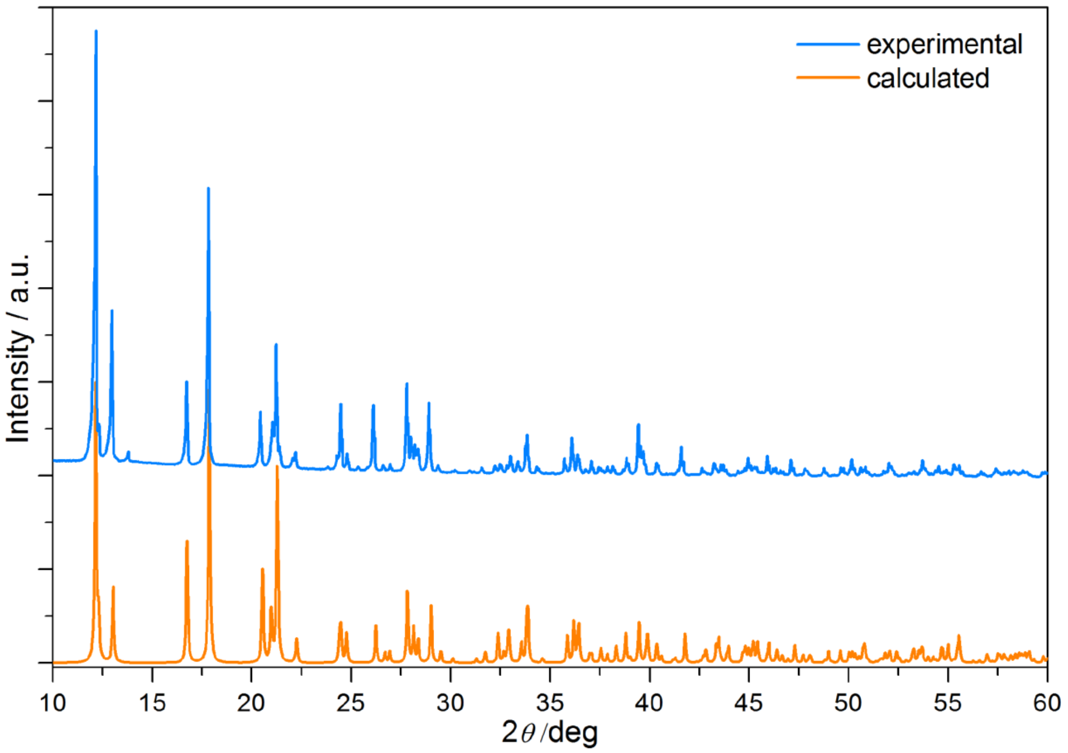

Figure S6. Experimental powder X-ray diffraction patterns of **1** (blue line) compared with the calculated pattern based on the single-crystal XRD structural model of **1** (orange line). The consequent small shift of all peaks between the experimental and the calculated patterns is due to the standard temperature effect, as the PXRD experiment was performed at room temperature when the single crystal X-ray diffraction measurement was executed at low temperature of 100(2) K (Table S1).

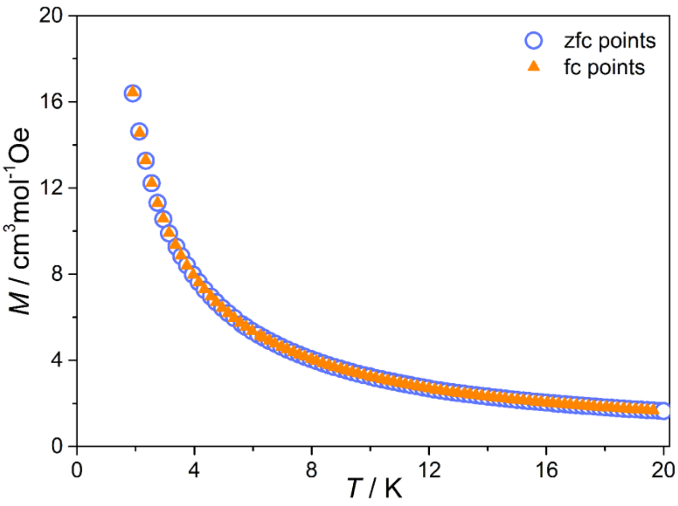

Figure S7. Zero-field cooled magnetization (ZFCM, light blue points) and field-cooled magnetization (FCM, orange points) curves of **1** measured at H_{dc} = 20 Oe. The lines are only to guide the eye.

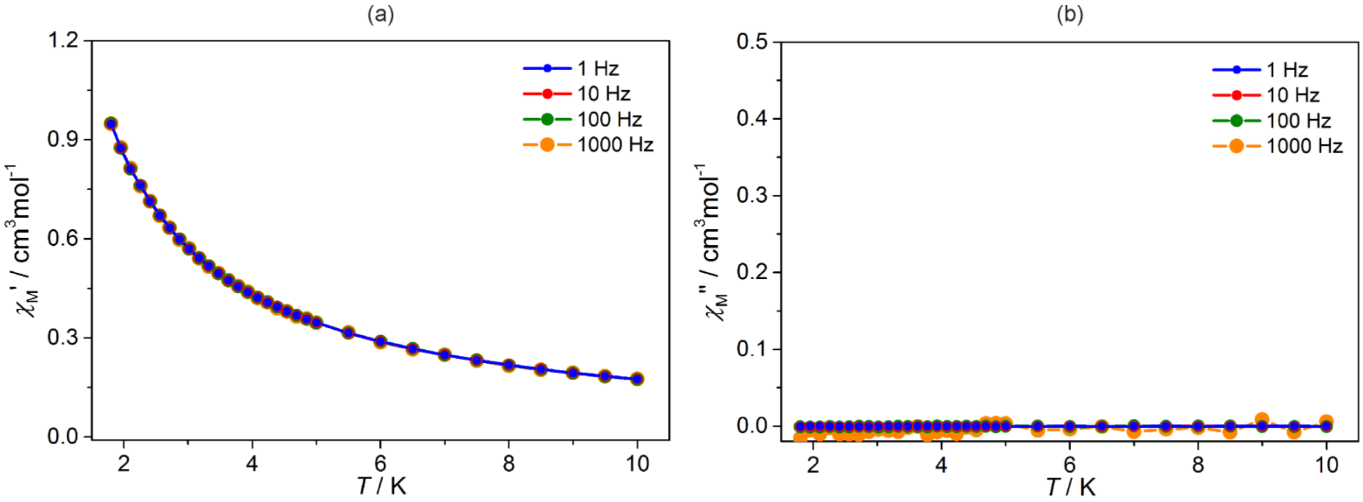

Figure S8. Alternate-current (*ac*) magnetic properties of **1** under zero direct-current (*dc*) magnetic field (H_{dc} = 0 Oe, H_{ac} = 1 Oe) in the form of temperature dependences of in-phase (χ_M', *a*) and out-of-phase (χ_M'', *b*) molar magnetic susceptibilities at various indicated frequencies of *ac* magnetic field. The solid lines are only to guide the eye.

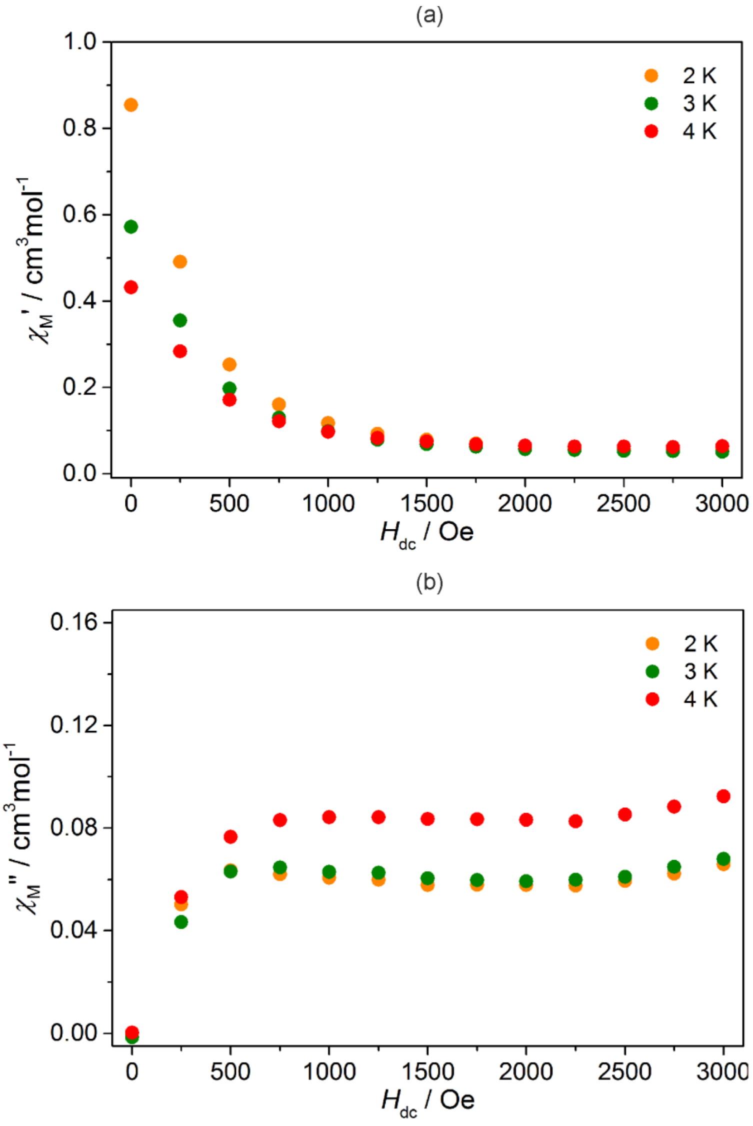

Figure S9. The dependence of in-phase (χ_M’, *a*) and out-of-phase (χ_M”, *b*) molar magnetic susceptibilities on the applied *dc* magnetic field from the 0–3000 Oe range at H_{ac} = 1 Oe and various indicated temperatures.

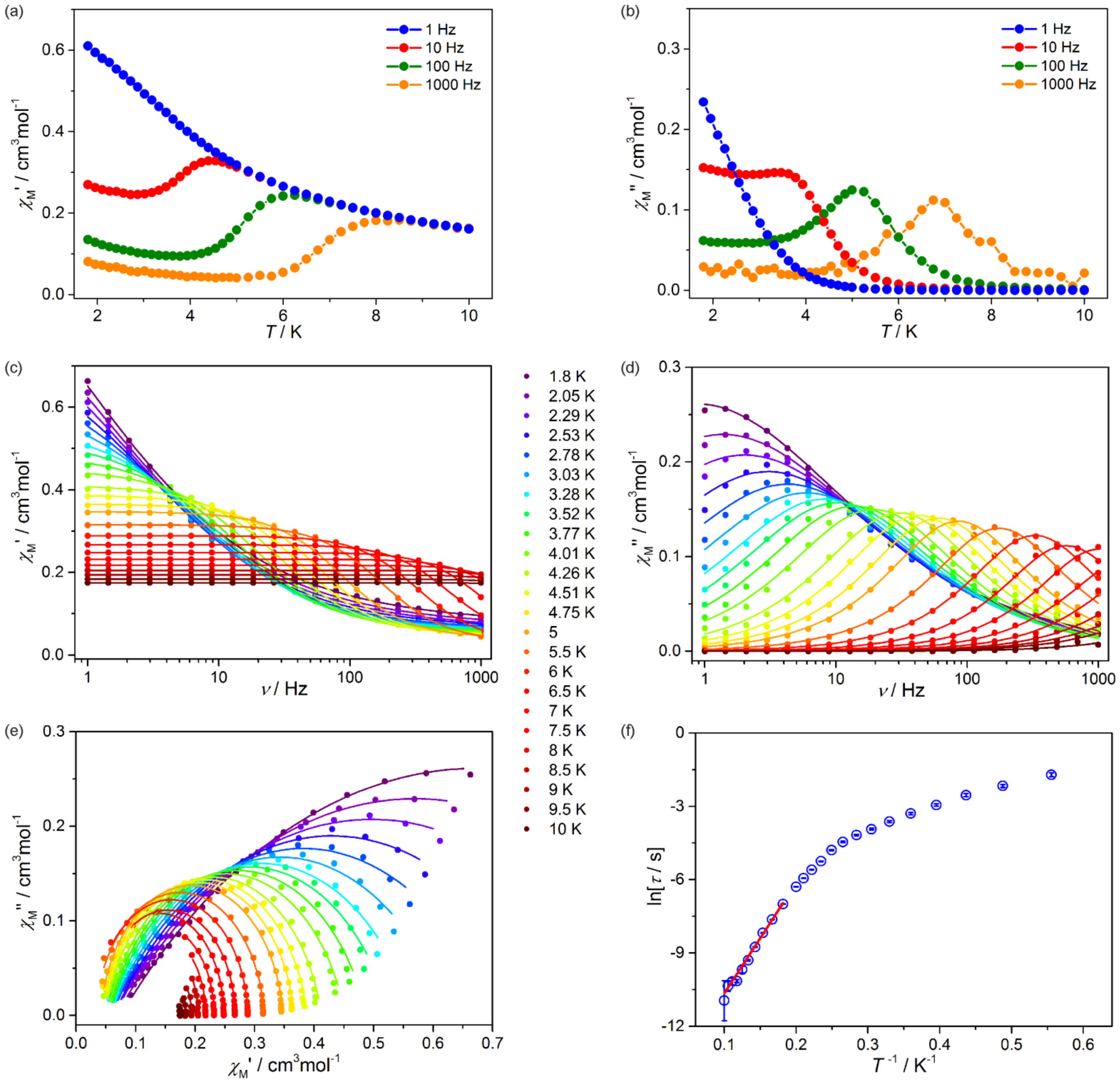

Figure S10. *AC* magnetic properties of **1** under *dc* field of 1000 Oe (H_{dc} = 1000 Oe, H_{ac} = 1 Oe): temperature dependences of in-phase χ_M’ (*a*) and out-of-phase χ_M” (*b*) molar magnetic susceptibility at various indicated frequencies of ac magnetic field, frequency dependences of χ_M’ (*c*) and χ_M” (*d*) susceptibilities at various indicated temperatures, the related Argand χ_M” – χ_M’ plots at the indicated temperatures (*e*), and the temperature dependence of the relaxation time, τ plotted as ln(τ) versus T^{-1} (*f*). The solid lines shown in (*c*-*e*) graphs represent the fittings according to the generalized Debye model (Table S4), while the solid line in (*f*) shows the linear fitting according to the Arrhenius law.

Table S4. Parameters obtained by fitting the Argand χ_M”–χ_M’ plots (H_{dc} = 1000 Oe, Figure S10) of **1** using the generalized Debye model.

T / K	χ_S cm^{3}mol^{-1}	χ_T cm^{3}mol^{-1}	***τ* / s**	*α*
1.80	0.075(3)	1.27(3)	**0.181(14)**	0.477(7)
2.05	0.067(3)	1.07(2)	**0.115(8)**	0.454(8)
2.29	0.063(3)	0.93(2)	**0.079(5)**	0.431(10)
2.53	0.063(3)	0.797(14)	**0.052(3)**	0.392(10)
2.78	0.059(3)	0.704(12)	**0.0371(17)**	0.361(12)
3.03	0.059(3)	0.627(9)	**0.0267(11)**	0.322(12)
3.28	0.058(3)	0.566(7)	**0.0195(7)**	0.282(13)
3.52	0.056(3)	0.528(6)	**0.0154(5)**	0.252(13)
3.77	0.055(3)	0.488(5)	**0.0116(3)**	0.215(12)
4.01	0.053(3)	0.542(4)	**0.0083(19)**	0.180(12)
4.26	0.049(2)	0.412(2)	**0.00526(10)**	0.137(10)
4.51	0.047(2)	0.389(2)	**0.00373(5)**	0.109(8)
4.75	0.044(2)	0.3661(12)	**0.00264(3)**	0.085(7)
5.0	0.041(2)	0.3476(9)	**0.00186(2)**	0.069(5)
5.5	0.033(2)	0.3157(7)	**0.000911(9)**	0.054(6)
6.0	0.0316(9)	0.2888(3)	**0.000485(3)**	0.031(3)
6.5	0.0413(13)	0.2668(3)	**0.000281(2)**	0.006(4)
7.0	0.034(2)	0.2478(2)	**0.000158(2)**	0.001(5)
7.5	0.036(5)	0.2319(2)	**0.000092(3)**	0.003(7)
8.0	0.043(19)	0.2172(4)	**0.000063(8)**	0
8.5	0.038(9)	0.2048(2)	**0.000039(2)**	0
9.0	0.077(17)	0.1939(2)	**0.000038(6)**	0
9.5	0.08(2)	0.1837(2)	**0.000032(7)**	0
10.0	0.09(7)	0.1748(2)	**0.000018(15)**	0

The following equations of the generalized Debye model for single relaxation process were applied:

$$\chi'(\omega) = \chi_S + (\chi_T - \chi_S)\frac{1 + (\omega\tau)^{1-\alpha}\sin\left(\pi\alpha/2\right)}{1 + 2(\omega\tau)^{1-\alpha}\sin\left(\pi\alpha/2\right) + (\omega\tau)^{2(1-\alpha)}}$$

$$\chi''(\omega) = (\chi_T - \chi_S)\frac{(\omega\tau)^{1-\alpha}\cos\left(\pi\alpha/2\right)}{1 + 2(\omega\tau)^{1-\alpha}\sin\left(\pi\alpha/2\right) + (\omega\tau)^{2(1-\alpha)}}$$

where

χ_S = the adiabatic susceptibility (at infinitely high frequency of *ac* field),

χ_T = the isothermal susceptibility (at infinitely low frequency of *ac* field),

τ = the relaxation time,

α = the distribution (Cole-Cole) parameter,

and $\omega = 2\pi\nu$, with ν being the frequency in [Hz] units.[S13-S14]

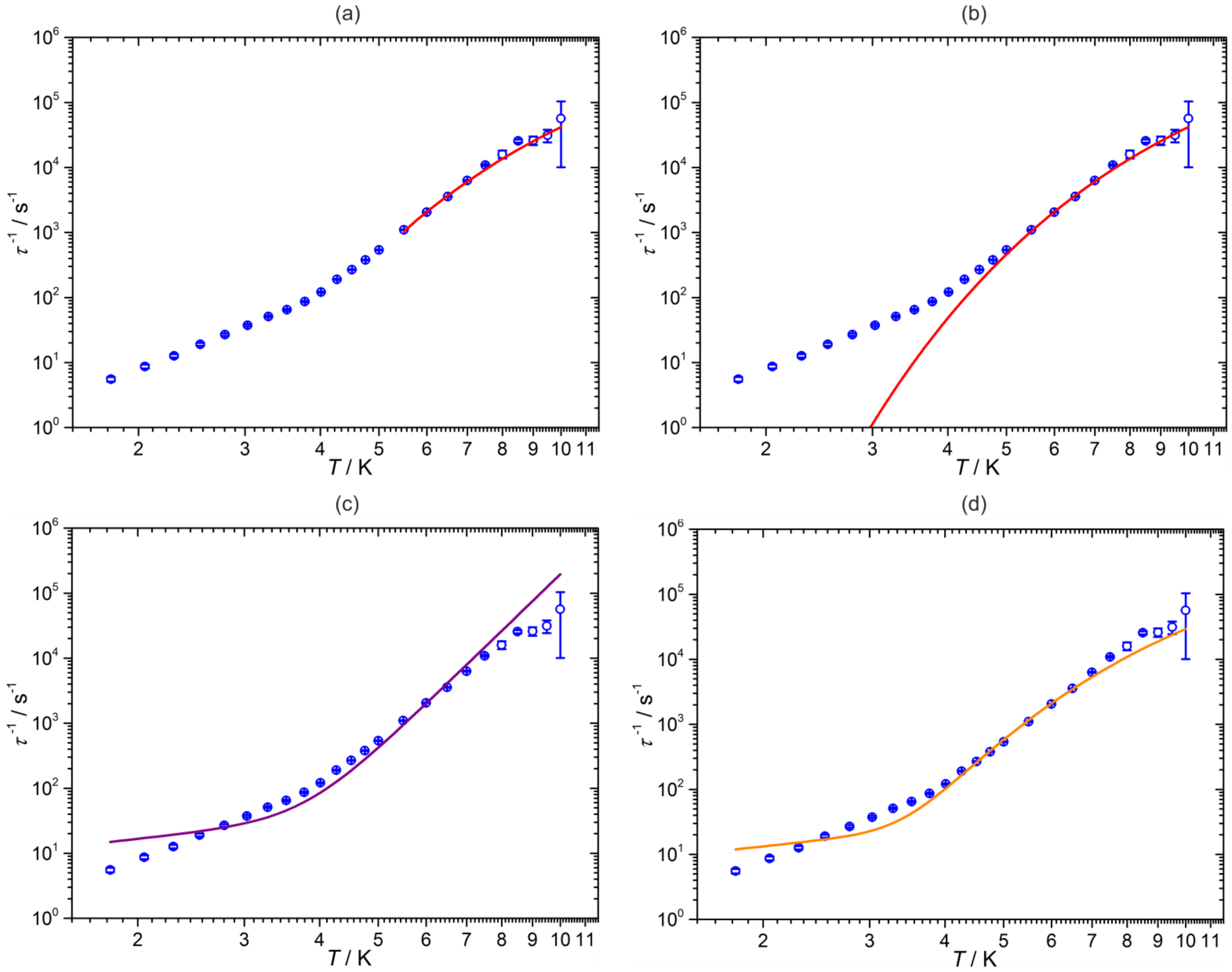

Figure S11. Temperature dependence of the inverse of the determined relaxation time of **1** (see Figure S10 and Table S4 for details, blue circles with the blue error bars) together with the various possible fittings : (*a*) according to the Arrhenius law, $\ln(\tau) = \Delta E/(k_BT) + \ln(\tau_0)$, where $\Delta E/k_B$ represent the effective thermal energy barrier, in the limited 5–10 K temperature range, (*b*) the Arrhenius law fitting for the limited 5–10 range with the extrapolation towards lower temperatures, (*c*) according to the equation: $\tau^{-1} = A_{dir}T + B_{Raman}T^9$ where the first term represents the contribution of one-phonon direct relaxation process dominant at low T, and the second term representing the two-phonon Raman process dominant at higher T,[S15] and (*d*) the mixed approach using the fitting using the Arrhenius equation term for the higher T range with the direct relaxation process dominant at low T, that is $\tau^{-1} = A_{dir}T + (1/\tau_0)\cdot\exp(-\Delta E/(k_BT))$. The best-fit parameters are: (*a*), (*b*) $\Delta E/k_B = 45(1)$ K, $\tau_0 = 2.6(5)\cdot10^{-7}$ s; (*c*) $A_{dir} = 8.3(5)$ s^{-1}K^{-1}, $B_{Raman} = 1.9(3)\cdot10^{-4}$ s^{-1}; (*d*) $A_{dir} = 6.6(5)$ s^{-1}K^{-1}, $\Delta E/k_B = 40(1)$ K, $\tau_0 = 6.4(5)\cdot10^{-7}$ s. Only the fitting according to the Arrhenius law for the limited temperature range of 5–10 K (*a*) gave the satisfactory agreement with the experimental data. This can be explained by the possibly more complex and multiple relaxation pathways existing in **1**. Thus, only the limited fitting according to the Arrhenius law could be reliably discussed, and it was presented in the manuscript (Figure 3).

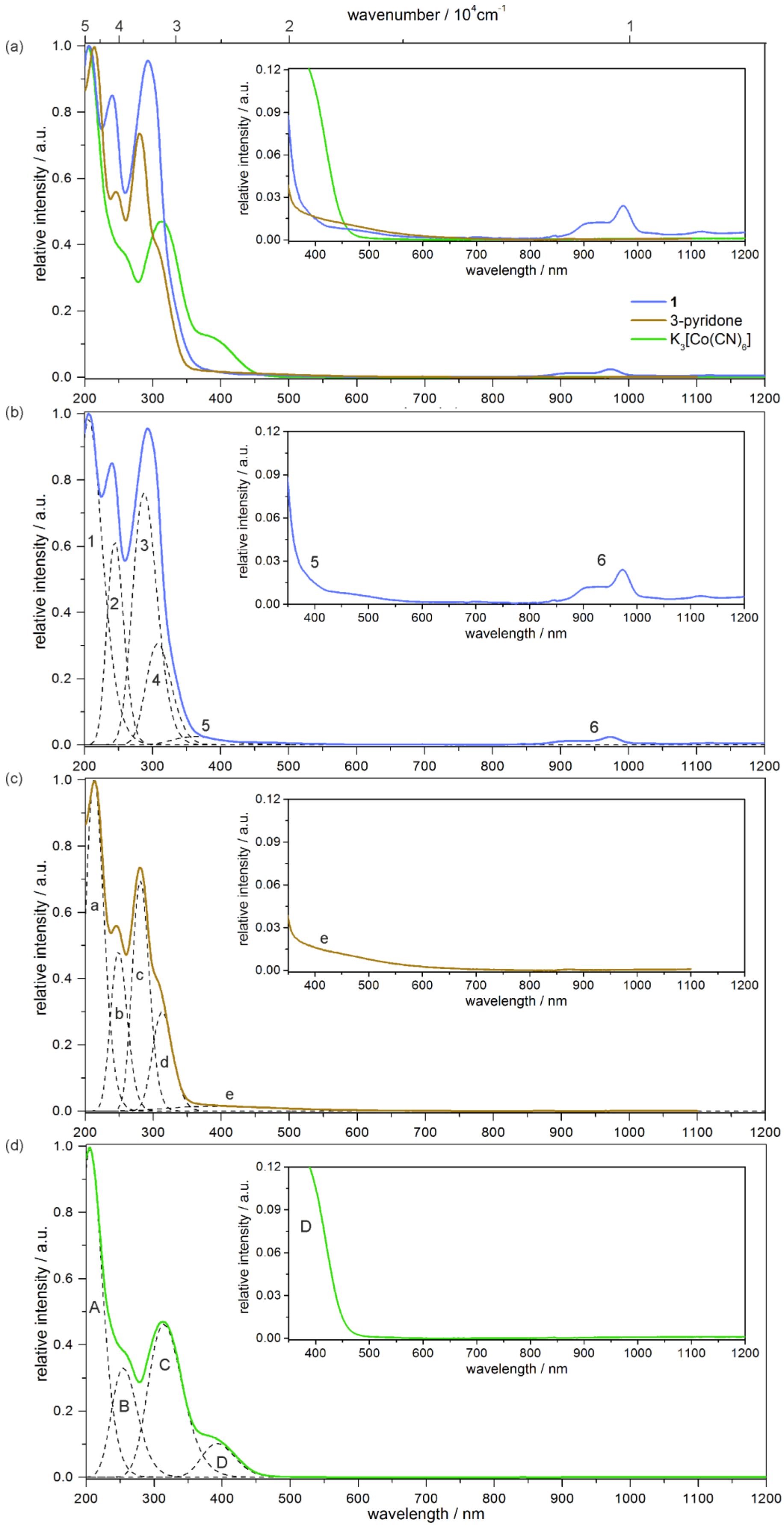

Figure S12. Solid state UV-Vis-NIR absorption spectra of **1** (*a*-*b*) compared with the spectra of 3-pyridone (*c*) and $K_3[Co(CN)_6]$ (*d*). Solid lines show the experimental data, dotted lines the deconvoluted components (see Table S5).

Table S5. Analysis of solid state UV-Vis-NIR absorption spectrum of **1** compared with the analyses of the relevant spectra of 3-pyridone and K$_3$[Co^{III}(CN)$_6$] (see Figure S11)

compound (figure)	peak no.	λ_{max} / nm	E_{max} / cm^{-1}	interpretation
1	1	206	48500	combined contribution from d-d of Co$^{III\text{-}LS}$: $^{1}A_{1g} \rightarrow {}^{1}E_{g}$, metal-to-ligand charge transfer (MLCT) of [Co^{III}(CN)$_6$]$^{3-}$, and singlet to singlet transition of 3-pyridone: $\pi \rightarrow \pi^*$
	2	245	40900	combined contribution from d-d of Co$^{III\text{-}LS}$: $^{1}A_{1g} \rightarrow {}^{1}T_{2g}$ and singlet to singlet transitions of 3-pyridone: $\pi \rightarrow \pi^*$
	3	287	34800	singlet to singlet transition of 3-pyridone: $\pi \rightarrow \pi^*$
	4	308	32500	combined contribution from d-d of Co$^{III\text{-}LS}$: $^{1}A_{1g} \rightarrow {}^{1}T_{1g}$ and singlet to triplet transition of 3-pyridone: $\pi \rightarrow \pi^*$
	5	362	27650	combined contribution from d-d of Co$^{III\text{-}LS}$: $^{1}A_{1g} \rightarrow {}^{3}T_{1g}$ and singlet to triplet transition of 3-pyridone: $\pi \rightarrow \pi^*$
	6	973	10280	f-f of Yb^{III}:[S16] $^{2}F_{7/2} \rightarrow {}^{2}F_{5/2}$
3-pyridone	a	213	46950	singlet to singlet transitionns:[S9,S17] $\pi \rightarrow \pi^*$
	b	249	40160	
	c	281	35600	
	d	313	31950	
	e	385	26000	singlet to triplet transition: $\pi \rightarrow \pi^*$
K$_3$[Co(CN)$_6$]	A	205	48700	d-d of Co$^{III\text{-}LS}$:[S4,S18-S21] $^{1}A_{1g} \rightarrow {}^{1}E_{g}$
	B	255	39240	d-d of Co$^{III\text{-}LS}$: $^{1}A_{1g} \rightarrow {}^{1}T_{2g}$ (minor contribution of $^{1}A_{1g} \rightarrow {}^{5}T_{2g}$)
	C	314	31830	d-d of Co$^{III\text{-}LS}$: $^{1}A_{1g} \rightarrow {}^{1}T_{1g}$ (minor contribution of $^{1}A_{1g} \rightarrow {}^{3}T_{2g}$)
	D	393	25470	d-d of Co$^{III\text{-}LS}$: $^{1}A_{1g} \rightarrow {}^{3}T_{1g}$

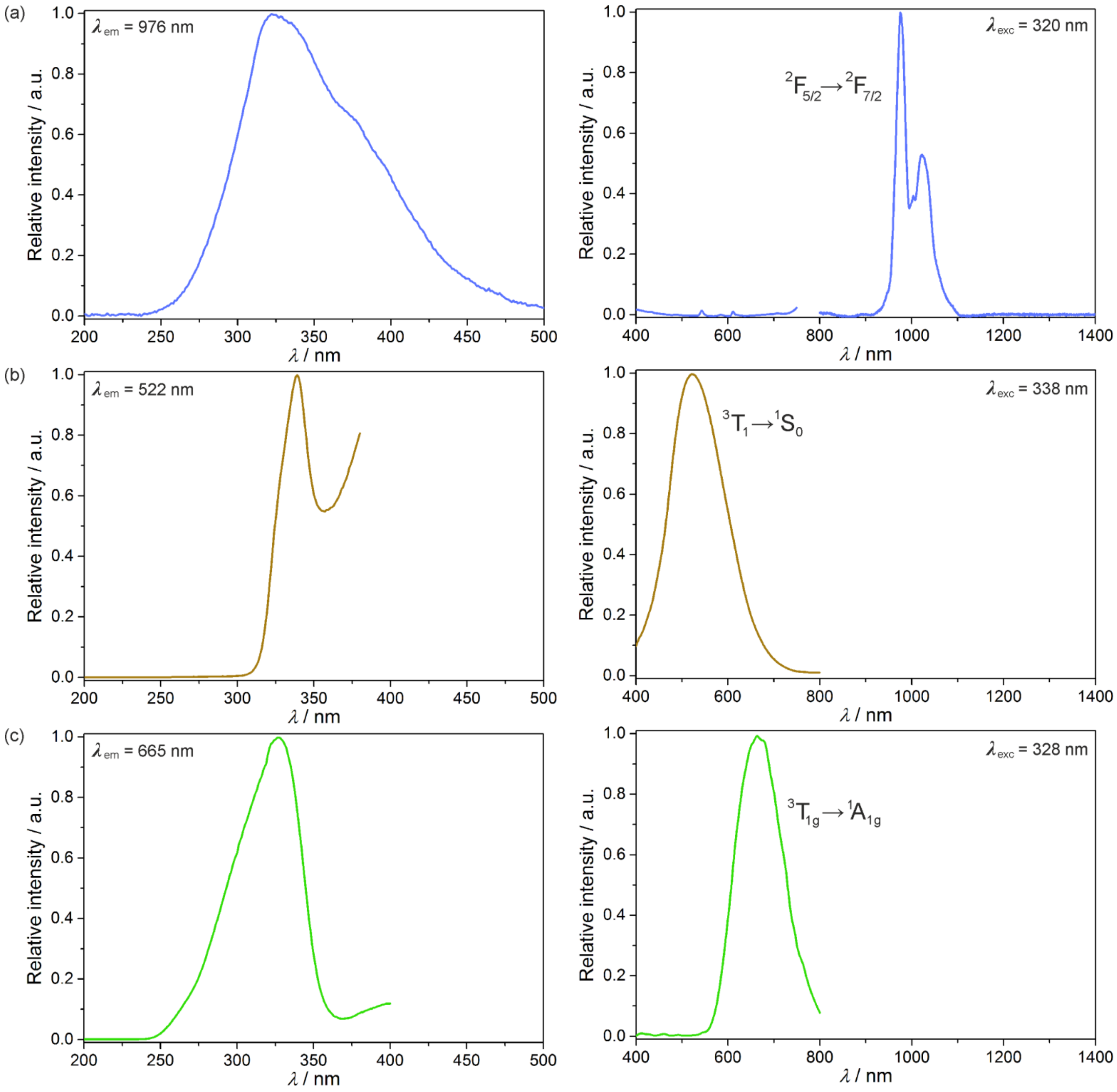

Figure S13. Room temperature solid state excitation (left panel) and emission (right panel) spectra of **1** (*a*) compared with the respective spectra of 3-pyridone (*b*) and $K_3[Co(CN)_6]$ (*c*). The excitation wavelengths for the emission spectra (λ_{exc}) and the monitored emission wavelengths (λ_{em}) for the excitation spectra are shown on the graphs. The electronic transitions related to the observed emission bands are also presented on the graphs.

Table S6. Summary of structural features, magnetic and optical properties of reported cyanido-bridged heterometallic assemblies containing Yb^{III} complexes

No.	**compound**	**structure**	**Yb^{III} C.N.**	**magnetic properties**	**optical properties**	**ref.**
1.	$\{[Yb^{III}(terpy)(dmf)_2(H_2O)_2][W^{V}(CN)_8]\}\cdot 3H_2O$	0D dinuclear	8	weak AF coupling	-	[S22]
2.	$\{[Yb^{III}(2,2'\text{-}bpy)_2(dmf)(H_2O)][Mo^{V}(CN)_8]\}\cdot 0.5(2,2'\text{-}bpy)\cdot 4.5H_2O$	1D chain	8	weak AF coupling	-	[S23]
3.	$\{[Yb^{III}(dmf)_6][Mo^{V}(CN)_8]\}$	1D chain	8	weak AF coupling	-	[S24]
4.	$\{[Yb^{III}(box)(dmf)_3][Mo^{V}(CN)_8]\}\cdot MeCN$	2D layer	8	weak interactions	Yb-based NIR emission; L to Yb ET	[S25]
5.	$[(n\text{-}C_4H_9)_4N]\{[Yb^{III}(phen)_2(H_2O)][Mo^{V}(CN)_8]\}[NO_3]\cdot 2MeCN\cdot 4H_2O$	1D chain	8	weak interactions	-	[S26]
6.	$[Hphen]_{2.5}\{[Yb^{III}_{0.5}(phen)(H_2O)][Mo^{IV}(CN)_8]\}\cdot 1.5MeCN$	0D trinuclear	8	-	-	[S26]
7.	$\{[Yb^{III}(H_2O)_2][Cr^{III}(CN)_6]\}\cdot 2H_2O$	3D network	8	-	-	[S27]
8.	$\{[Yb^{III}(2,2'\text{-}bpy)(H_2O)_4][Cr^{III}(CN)_6]\}\cdot 1.5(2,2'\text{-}bpy)\cdot 3.5H_2O$	1D chain	8	-	-	[S28
9.	$\{[Yb^{III}(dmf)_4(H_2O)_2][Cr^{III}(CN)_6]\}\cdot H_2O$	1D chain	8	-	Yb-based NIR emission; Cr to Yb ET	[S20]
10.	$\{[Yb^{III}_3Cr^{III}_2(CH_3COO)_6(OH)_6(H_2O)_6][Cr^{III}(CN)_6]\}\cdot 4(4,4'\text{-}bpy)\cdot 13H_2O$	0D ionic	8	-	-	[S29]
11.	$\{[Yb^{III}(H_2O)_2][Co^{III}(CN)_6]\}\cdot 2H_2O$	3D network	8	-	-	[S30]
12.	$\{[Yb^{III}(dmf)_4(H_2O)_3][Co^{III}(CN)_6]\}\cdot 2H_2O$	0D dimer	8	-	-	[S31]
13.	$\{[Yb^{III}(2,2'\text{-}bpy)(H_2O)_4][Co^{III}(CN)_6]\}\cdot 1.5(2,2'\text{-}bpy)\cdot 4H_2O$	1D chain	8	-	-	[S32]
14.	$\{[Yb^{III}(dmf)_4(H_2O)_3][Cr^{III}(CN)_6]\}\cdot H_2O$	0D dinuclear	8	-	Yb-based NIR emission; Co to Yb ET	[S20]
15.	$\{[Yb^{III}(H_2O)_2][Fe^{III}(CN)_6]\}\cdot 2H_2O$	3D network	8	antiferro-magnet, $T_N = 1.8$ K	-	[S27]
16.	$A\{[Yb^{III}(H_2O)_3][Fe^{II}(CN)_6]\}\cdot 0.5H_2O$ (A = K, Rb, NH_4, Tl, Cs)	3D network	9	-	-	[S33]
17.	$Yb^{III}_4[M^{II}(CN)_6]_3\cdot nH_2O$ (M = Fe, Ru)	3D network	8 and 9	-	-	[S34]
18.	$\{[Yb^{III}(phen)_2(H_2O)_2][Fe^{III}(CN)_6]\}\cdot 2(phen)$	1D chain	8	-	-	[S35]
19.	$\{[Yb^{III}(dmf)_4(H_2O)_3][Fe^{III}(CN)_6]\}\cdot nH_2O$	0D dinuclear	8	-	-	[S31, S36, S37]
20.	$\{[Yb^{III}(2,2'\text{-}bpy)(H_2O)_4][Fe^{III}(CN)_6]\}\cdot 1.5(2,2'\text{-}bpy)\cdot 4H_2O$	1D chain	8	weak interactions	-	[S32]
21.	$\{[Yb^{III}_2(dma)_5(H_2O)_5][Fe^{III}(CN)_6]_2\}\cdot 2H_2O$	0D tetranuclear	7	-	-	[S38]
22.	$\{[Yb^{III}(dmso)_4(H_2O)][Fe^{III}(CN)_6]\}$	1D chain	7	-	-	[S39]
23.	$\{[Yb^{III}(deso)_2(H_2O)_3][Fe^{III}(CN)_6]\}\cdot 2H_2O$	1D chain	7	-	-	[S39]
24.	$\{[Yb^{III}(tmso)_2(H_2O)_3][Fe^{III}(CN)_6]\}\cdot H_2O$	1D chain	7	-	-	[S39]
25.	$\{[Yb^{III}(dmf)_6][Fe^{III}(CN)_6]\}$	1D chain	8	-	-	[S40]
26.	$K\{[Yb^{III}(H_2O)_3][M^{II}(CN)_6]\}\cdot H_2O$ (M = Ru, Os)	3D network	8	-	-	[S41]

27.	$\{[Yb^{III}(dmf)_5]_2[Ni^{II}(CN)_4]_3\}$	1D chain	8	-	-	[S42]
28.	$\{[Yb^{III}(dmf)_5]_2[M^{II}(CN)_4]_3\}$ (M = Pt, Pd)	1D chain	8	-	-	[S42, S43]
29.	$\{[Yb^{III}(Cl)(dma)_4][Ni^{II}(CN)_4]\}$	1D chain	7	-	-	[S44]
30.	$\{[K_2(dmf)_4][Pt^{II}(CN)_4]\}\{[Yb^{III}_2(dmf)_{10}[Pt^{II}(CN)_4]\}$	2D layer	8	-	-	[S44]
31.	$[NH_4]\{[Yb^{III}(dmf)_4][Pt^{II}(CN)_4]_2\}$	1D chain	8	-	-	[S44]
32.	$[Yb^{III}(terpy)(dmf)_2(H_2O)_2(NO_3)][Pt^{II}(CN)_4]$	0D ionic salt	9	-	-	[S45]
33.	$\{[Yb^{III}(terpy)(H_2O)_2(NO_3)][Pt^{II}(CN)_4]\}\cdot 0.5MeCN\cdot 1.5H_2O$	1D chain	9	-	-	[S46]
34.	$\{[Yb^{III}(terpy)(H_2O)_2(NO_3)][Pt^{II}(CN)_4]\}\cdot MeCN$	1D chain	9	-	-	[S47]
35.	$\{[Yb^{III}_6(dmf)_{16}(O)(OH)_8][Pd^{II}(CN)_4]\}[Pd^{II}(CN)_4]_3\cdot 4(dmf)$	1D chain	8	-	-	[S48]
36.	$\{[Yb^{III}(dmso)_3(H_2O)(NO_3)][Pt^{II}(CN)_4]\}$	1D chain	8	-	-	[S49]
37.	$\{[Yb^{III}(phen)(dmso)_2(H_2O)_3]_2[Pt^{II}(CN)_4]\}[Pd^{II}(CN)_4]_2 \cdot 2(phen)\cdot 4H_2O$	0D trinuclear	8	-	-	[S50]
38.	$\{[Yb^{III}(tpp)(dmf)_2]_2[M^{II}(CN)_4]\}$ (M = Ni, Pt)	0D trinuclear	7	-	-	[S51]
39.	$\{[Yb^{III}(terpy)(H_2O)(NO_3)_2][Au^{I}(CN)_2]\}$	0D dinuclear	9	-	-	[S52]
40.	$[K(H_2O)_4]\{[Yb^{III}(H_2O)_6][Ru^{II}(bpy)(CN)_4]\}\cdot 5H_2O$	0D trinuclear	8	-	Yb-based NIR emission; Ru to Yb ET	[S53, S57]
41.	$\{[Yb^{III}(H_2O)_6][Ru^{II}(bpy)(CN)_4]\}[Ru^{II}(bpy)(CN)_4]\cdot 13H_2O$	1D chain	8	-	Ru-based red emission	[S53]
42.	$\{[Yb^{III}(NO_3)(H_2O)_2][Yb^{III}(NO_3)_{0.5}(H_2O)_{5.5}][Ru^{II}(bpym)(CN)_4]\}[NO_3]_{0.5}\cdot 5.5H_2O$	2D layer	8	-	Yb-based NIR emission; Ru to Yb ET	[S54]
43.	$\{[Yb^{III}(H_2O)_6]_{0.5}[Yb^{III}(H_2O)_4][Ru^{II}(bpym)(CN)_4]_2\}[NO_3]_{0.5}\cdot 8H_2O$	3D network	7 and 8	-	Yb-based NIR emission; bpym to Yb ET	[S54]
44.	$K_2\{[Yb^{III}(phen)_2(H_2O)][Ru^{II}(phen)(CN)_4]_2\}_2\cdot 28H_2O$	0D hexanculear	8	-	Yb-based NIR emission; Ru to Yb ET	[S55, S56]
45.	$\{[Yb^{III}(phen)(H_2O)_3]_2[Ru^{II}(phen)(CN)_4]_3\}\cdot 14H_2O$	2D layer	8	-	Yb-based NIR emission; Ru to Yb ET	[S56]
46.	$\{[Yb^{III}_2(bpym)(H_2O)_7][Ru^{II}(phen)(CN)_4]_3\}\cdot n$(solvent)	1D chain	8	-	Yb-based NIR emission; Ru to Yb ET	[S56]

Abbreviations: C.N. = coordination number, ET = energy transfer, NIR = near-infrared, terpy = 2,2′:6′,2″-terpyridine; dmf = N,N’-dimethylformamide, box = 2,2’-bis(2-oxazoline), 2,2’-bpy = 2,2’-bipyridine, phen = 1,10-phenanthroline, dma = N,N’-dimethylacetamide, dmso = dimethyl sulfoxide, deso = diethyl sulfoxide; tmso = tetramethylene sulfoxide; tpp = tetraphenylporphyrinate dianion; bpym = 2,2’-bipyrimidine.

References to Supporting Information

[S1] W.-T. Chen, G.-C. Guo, M.-S. Wang, G. Xu, L.-Z. Cai, T. Akitsu, M. Akita-Tanaka, A. Matsuchita and J.-S. Huang, *Inorg. Chem.*, 2007, **46**, 2105.

[S2] W.-T. Chen, A.-Q. Wu, G.-C. Guo, M.-S. Wang, L.-Z. Cai and J.-S. Huang, *Eur. J. Inorg. Chem.*, 2010, 2826.

[S3] Y. Zhang, Z. Guo, S. Xie, H.-L. Li, W.-H. Zhu, L. Liu, X.-Q. Dong, W.-X. Ren, L.-Z. Liu and A. K. Powell, *Inorg. Chem.*, 2015, **54**, 10316.

[S4] S. Chorazy, M. Rams, K. Nakabayashi, B. Sieklucka and S. Ohkoshi, *Chem. Eur. J.*, 2016, **22**, 7371.

[S5] O. Castillo, A. Luque, S. Iglesias, P. Vitoria and P. Roman, *New. J. Chem.*, 2000, **24**, 771.

[S6] B. Kozlevcar, L. Glazar, G. Pirc, Z. Jaglicic, A. Golobic and P. Segedin, *Polyhedron*, 2007, **26**, 11.

[S7] G. M. Sheldrick, *Acta Crystallogr.*, 2008, **A64**, 112.

[S8] L. J. Farrugia, *J. Appl. Cryst.*, 2012, **45**, 849.

[S9] O. K. Abou-Zied and O. I. K. Al-Shihi, *Phys. Chem. Chem. Phys.*, 2009, **11**, 5377.

[S10] C. F. Macrae, I. J. Bruno, J. A. Chisholm, P. R. Edgington, P. McCabe, E. Pidcock, L. Rodriguez-Monge, R. Taylor, J. van der Streek and P. A. Wood, *J. Appl. Crystallogr.*, 2008, **41**, 466.

[S11] M. Llunell, D. Casanova, J. Cirera, J. Bofill, P. Alemany, S. Alvarez, M. Pinsky, D. Avnir, *SHAPE v. 2.1. Program for the Calculation of Continuous Shape Measures of Polygonal and Polyhedral Molecular Fragments*, University of Barcelona: Barcelona, Spain, 2013.

[S12] D. Casanova, J. Cirera, M. Llunell, P. Alemany, D. Avnir and S. Alvarez, *J. Am. Chem. Soc.*, 2004, **126**, 1755.

[S13] Y.-N. Guo, G.-F. Xu, Y. Guo and J. Tang, *Dalton Trans.*, 2011, **40**, 9953.

[S14] M. Ramos Silva, P. Martin-Ramos, J. T. Coutinho, L. C. J. Pereira and J. Martin-Gil, *Dalton Trans.*, 2014, **43**, 6752.

[S15] S. Gomez-Coca, A. Urtizberea, E. Cremades, P. J. Alonso, A. Camon, E. Ruiz and F. Luis, *Nat. Commun.*, 2014, **5**, 4300.

[S16] W. Fan, Z. Zhang, L. Chen and L. Lu, *CrystEngComm*, 2015, **17**, 1881.

[S17] A. Weisstuch, P. Neidig and A. C. Tesla, *J. Lumin.*, 1975, **10**, 137.

[S18] V. M. Miskowski, H. B. Gray, R. B. Wilson and E. I. Solomon, *Inorg. Chem.*, 1979, **18**, 1410.

[S19] H. Kunkely and A. Vogler, Inorg. *Chem. Commun.*, 2004, **7**, 770.

[S20] T. Lazarides, G. M. Davies, H. Adams, C. Sabatini, F. Barigelletti, A. Barbieri, S. J. A. Pope, S. Faulkner and M. D. Ward, *Photochem. Photobiol. Sci.*, 2007, **6**, 1152.

[S22] S. Chorazy, J. Wang and S. Ohkoshi, *Chem. Commun.*, 2016, **52**, 10795.

[S22] P. Przychodzeń, R. Pełka, K. Lewiński, J. Supel, M. Rams, K. Tomala and B. Sieklucka, *Inorg. Chem.*, 2007, **46**, 8924.

[S23] S.-L. Ma, S. Ren, Y. Ma, D.-Z. Liao and S.-P. Yan, *J. Inorg. Organomet. Polym.*, 2010, **20**, 229.

[S24] Y.-Z. Tong, Q.-L. Wang, C.-Y. Su, Y. Ma, S. Ren, G.-F. Xu, G.-M. Yang, P. Cheng and D.-Z. Liao, *CrystEngComm*, 2013, **15**, 9906.

[S25] S. Chorazy, M. Arczynski, K. Nakabayashi, B. Sieklucka and S. Ohkoshi, *Inorg. Chem.*, 2015, **54**, 4724.

[S26] H. Zhou, Q. Chen, H.-B. Zhou, X.-Z. Yang, Y. Song and A.-H. Yuan, *Cryst. Growth Des.*, 2016, **16**, 1708.

[S27] F. Hulliger, M. Landolt and H. Vetsch, *J. Solid State Chem.*, 1976, **18**, 283.

[S28] M. Estrader, J. Ribas, V. Tangoulis, X. Solans, M. Font-Bardla, M. Maestro and C. Diaz, *Inorg. Chem.*, 2006, **45**, 8239.

[S29] S. K. Ma and S. Ren, *Rus. J. Coord. Chem.*, 2012, **38**, 253.

[S30] F. Hulliger, M. Landolt and H. Vetsch, *J. Solid State Chem.*, 1976, **18**, 307.

[S31] A. Figuerola, C. Diaz, J. Ribas, V. Tangoulis, J. Granell, F. Lloret, J. Mahia and M. Maestro, *Inorg. Chem.*, 2003, **42**, 641.

[S32] A. Figuerola, C. Diaz, J. Ribas, V. Tangoulis, C. Angregorio, D. Gatteschi, M. Maestro and J. Mahia, *Inorg. Chem.*, 2003, **42**, 5274.

[S33] D. F. Mullica, E. L. Sappenfield and T. A. Cunningham, *J. Solid State Chem.*, 1991, **91**, 98.

[S34] F. Hulliger, H. Vetsch, V. Gramlich and X.-L. Xu, *J. All. Comp.*, 1994, **207/208**, 192.

[S35] M. Katada, T. Nawa, H. Kumagai, S. Kawata and S. Kitagawa, *J. Radioanal. Nucl. Chem.*, 1999, **239**, 227.

[S36] D. F. Mullica, J. M. Farmer, B. P. Cunningham and J. A. Kautz, *J. Coord. Chem.*, 2000, **49**, 239.

[S37] H. Svendsen, M. R. V. Jorgensen, J. Overgaard, Y.-S. Chen, G. Chastanet, J.-F. Letard, K. Kato, M. Takata and B. B. Iversen, *Inorg. Chem.*, 2011, **50**, 10794.

[S38] H. Svendsen, J. Overgaard, M. A. Chevalier and B. B. Iversen, *Acta Cryst.*, 2006, **E62**, m793.

[S39] J.-R. Li, W.-T. Chen, M.-L. Tong, G.-C. Guo, Y. Tao, Q. Yu, W.-C. Song and X.-H. Bu, *Cryst. Growth Des.*, 2008, **8**, 2780.

[S40] D. C. Wilson, S. Liu, X. Chen, E. A. Meyers, X. Bao, A. V. Prosvirin, K. R. Dunbar, C. M. Hadad and S. G. Shore, *Inorg. Chem.*, 2009, **48**, 5725.

[S41] X. Xu and F. Hulliger, *Eur. J. Solid State Inorg. Chem.*, 1991, **28**, 625.

[S42] D. W. Knoeppel and S. G Shore, *Inorg. Chem.*, 1996, **35**, 1747.

[S43] D. W. Knoeppel, J. Liu, E. A. Meyers and S. G. Shore, *Inorg. Chem.*, 1998, **37**, 4828.

[S44] B. Du, E. A. Meyers and S. G. Shore, *Inorg. Chem.*, 2001, **40**, 4353.

[S45] M. Stojanovic, N. J. Robinson, X. Chen, P. A. Smith and R. E. Sykora, *J. Solid State Chem.*, 2010, **183**, 933.

[S46] B. A. Maynard, P. A. Smith, A. Jaleel, L. Ladner and R. E. Sykora, *J. Chem. Crystallogr.*, 2010, **40**, 616.

[S47] P. A. Smith, M. Stojanovic and R. E. Sykora, *Acta Cryst.*, 2010, **E66**, m1619.

[S48] J. Liu, E. A. Meyers and S. G. Shore, *Inorg. Chem.*, 1998, **37**, 5410.

[S49] M. Stojanovic, N. J. Robinson, Z. Assefa and R. E. Sykora, *Inorg. Chim. Acta*, 2011, **376**, 414.

[S50] M. Stojanovic, N. J. Robinson, X. Chen and R. E. Sykora, *Inorg. Chem. Acta*, 2011, **370**, 513.

[S51] X. Zhu, W.-K. Wong, J. Gou, W.-Y. Wong and J.-P. Zhang, *Eur. J. Inorg. Chem.*, 2008, 3515.

[S52] F. White, L. M. Pham, K. R. Xiang, R. Thomas, P. Vogel, C. Crawford, Z. Assefa and R. E. Sykora, *Inorg. Chem. Acta*, 2014, **414**, 240.

[S53] T. A. Miller, J. C. Jeffery, M. D. Ward, H. Adams, S. J. A. Pope and S. Faulkner, *Dalton Trans.*, 2004, 1524.

[S54] J.-M. Herrera, S. J. A. Pope, H. Adams, S. Faulkner and M. D. Ward, *Inorg. Chem.*, 2006, **45**, 3895.

[S55] S. G. Baca, H. Adams and M. D. Ward, *CrystEngComm*, 2006, **8**, 635.

[S56] S. G. Baca, H. Adams, D. Sykes, S. Faulkner and M. D. Ward, *Dalton Trans.*, 2007, 2419.

[S57] G. M. Davies, S. J. A. Pope, H. Adams, S. Faulkner and M. D. Ward, *Inorg. Chem.*, 2005, **44**, 4656.